Article

Overwintering fires in boreal forests

https://doi.org/10.1038/s41586-021-03437-y

Received: 16 July 2020

Accepted: 9 March 2021

Published online: 19 May 2021

Check for updates

Rebecca C. Scholten[1]✉, Randi Jandt[2], Eric A. Miller[3], Brendan M. Rogers[4] & Sander Veraverbeke[1]

Forest fires are usually viewed within the context of a single fire season, in which weather conditions and fuel supply can combine to create conditions favourable for fire ignition—usually by lightning or human activity—and spread[1–3]. But some fires exhibit 'overwintering' behaviour, in which they smoulder through the non-fire season and flare up in the subsequent spring[4,5]. In boreal (northern) forests, deep organic soils favourable for smouldering[6], along with accelerated climate warming[7], may present unusually favourable conditions for overwintering. However, the extent of overwintering in boreal forests and the underlying factors influencing this behaviour remain unclear. Here we show that overwintering fires in boreal forests are associated with hot summers generating large fire years and deep burning into organic soils, conditions that have become more frequent in our study areas in recent decades. Our results are based on an algorithm with which we detect overwintering fires in Alaska, USA, and the Northwest Territories, Canada, using field and remote sensing datasets. Between 2002 and 2018, overwintering fires were responsible for 0.8 per cent of the total burned area; however, in one year this amounted to 38 per cent. The spatiotemporal predictability of overwintering fires could be used by fire management agencies to facilitate early detection, which may result in reduced carbon emissions and firefighting costs.

Arctic-boreal regions are warming faster than the global average[7,8], and are estimated to store more than twice as much carbon as the Earth's atmosphere in their organic soils[9]. Fires are a natural disturbance in boreal forests, and release carbon from above- and belowground carbon pools into the atmosphere. A large fraction of the carbon emissions from fires in northern high latitudes originates from belowground carbon pools, as these fires often burn deep into organic soils[10–12]. In a warming climate, boreal fire regimes are intensifying and fires may burn deeper into organic soils and thereby threaten soil carbon reservoirs[10,13]. Moreover, increasing summer temperatures in northern high latitudes lead to more severe 'fire weather'[14] (that is, the atmospheric temperature, moisture and wind conditions that describe fire potential) and more lightning ignitions[2] that enable fires to burn over a greater area. However, regional differences in decadal burned-area trends exist and the relatively short length of consistent burned-area time series influences the interpretation[15]. Containment expenses increase exponentially with fire size, and therefore large fires constitute the majority of the budget allocated to fire management agencies in the USA and Canada[16,17]. The stagnant fire management budgets[18] in the USA and Canada are under pressure because of the increasing threats of climate warming and continued expansion of dwellings into the wildland–urban interface. Prevention and aggressive initial attack on undesired fires may be a viable way to lower firefighting costs[16,18].

Traditionally, the fire season in high latitudes begins with the lightning season in June or early-season human activities like debris burning[2,3,19]. Once ignited, boreal fires can smoulder in organic soils during periods when weather does not favour flaming spread, and, after days or months, re-emerge under weather conditions that favour flaming[1,20,21]. Smouldering boreal fires often remain undetected, especially in remote areas, which poses challenges for fire managers[1]. Recently, fire managers in Alaska, USA, and the Northwest Territories, Canada, started reporting an increasing number of extreme manifestations of this holdover phenomenon. In such cases, some fires 'hibernate' in deep organic soil layers for seven to eight months during the winter and re-emerge early the next fire season, in what can appear to be a new ignition. Limited and often anecdotal evidence of these overwintering fires exists in recent Alaskan fire management reports and operating plans[22,23], as well as news reports[24]. Overwintering ('zombie') fires are an understudied phenomenon in boreal forests and may have severe implications for fire management, human health and climate[4,5].

Detection of large overwintering fires

Overwintering fires typically undergo four temporal stages. Towards the end of a fire season, the fire seemingly stops burning as flaming spread ceases (Fig. 1a). Unnoticed, it smoulders during winter under the snow cover (Fig. 1b). As soon as fire weather facilitates fire spread in the following fire season, the fire flames up (Fig. 1c, Extended Data Fig. 1), thereby burning additional area (Fig. 1d). This sequence of events allows for the identification of spatial and temporal characteristics of overwintering fires. First, newly burned areas of an overwintering fire are found near the original burn scar, and second, they require no additional ignition source and can therefore re-emerge early in the fire season, before the main lightning season.

We developed an algorithm to retrospectively identify and map overwintering fires based on these two spatiotemporal characteristics

[1]Faculty of Science, Vrije Universiteit Amsterdam, Amsterdam, The Netherlands. [2]Alaska Fire Science Consortium, University of Alaska, Fairbanks, AK, USA. [3]Bureau of Land Management, Alaska Fire Service, Fort Wainwright, AK, USA. [4]Woodwell Climate Research Center, Falmouth, MA, USA. ✉e-mail: r.c.scholten@vu.nl

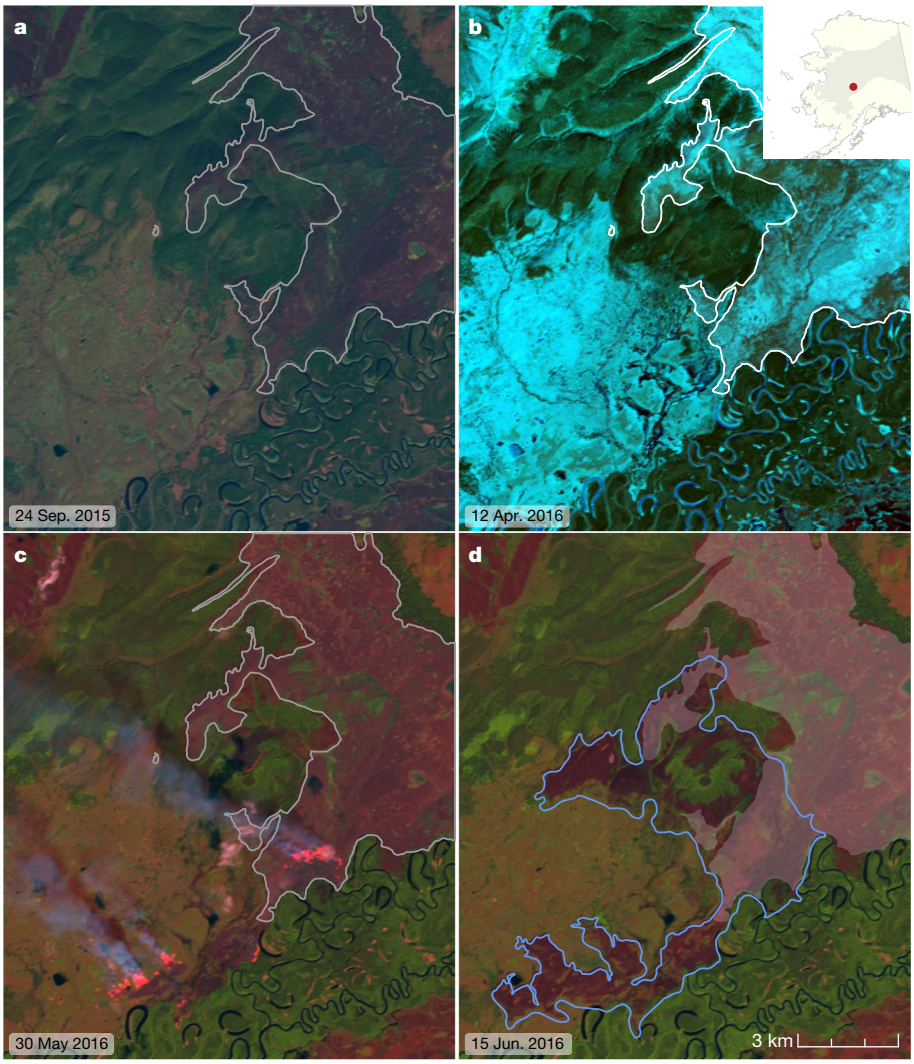

Fig. 1 | Landsat 8 false-colour time series of a 2015 fire in Alaska that generated an overwintering fire in 2016. a, 24 September 2015; **b**, 12 April 2016 (study area shown in inset); **c**, 30 May 2016; and **d**, 15 June 2016 (scale at the bottom right). A burn scar at the end of the fire season (white perimeter, **a**) had seemingly extinguished but was smouldering under the snow layer (**b**) until favourable conditions enabled the fire to re-emerge (**c**), thereby creating additional burned area (blue perimeter, **d**). Fire perimeters were taken from the Alaska Large Fire Database. The Landsat composites used the spectral bands centred at 2.20 µm (red), 0.86 µm (green) and 0.65 µm (blue). Imagery was plotted in R. Inset map made with Natural Earth.

(Extended Data Fig. 2). We analysed the locations of 45 small overwintering fires reported by fire managers in Alaska and the Northwest Territories between 2005 and 2017 to determine a suitable threshold for the distance between a holdover and its fire of origin. We define 'small fires' to be those whose re-emergence remained undetected in the Moderate Resolution Imaging Spectroradiometer (MODIS) active fire product[25]. Small overwintering fire sizes ranged from 0.04 ha to 42.5 ha, and 78% of the fires burned less than 1 ha. We found that 89% of these small overwintering fires started within the fire perimeter from the year before, and 93% travelled less than 500 m over the winter (Extended Data Fig. 3). Our results are consistent with laboratory experiments on boreal peat, which have shown that smouldering fires spread at a rate of around 100–250 m yr^{-1} (10–30 mm h^{-1}), depending on oxygen supply and the water and mineral contents of the peat[6]. We therefore adopted a threshold of 1,000 m to search for overwintering flare-ups in the vicinity of burned area from the year before. The 1,000-m threshold was chosen because it is the approximate nadir pixel size of the MODIS active fire product that we used to detect fires.

In Alaska and the Northwest Territories, fine fuels consisting of grass and litter are conducive to flaming spread as early as mid- to late May, even before convective thunderstorm activity starts[26]. The timing of dry fuel availability is dependent on the onset of snow melt in spring, which varies in time and space[23]. Spring snow melt is dependent on winter and spring temperatures and precipitation, and is therefore a suitable proxy of spring and winter weather conditions; it has also been shown to be an effective predictor of fire activity[27]. To capture the annual variability in dry fuel availability, we based the temporal constraint of our algorithm on the regional yearly snowmelt onset day, which we calculated from the MODIS daily fractional snow cover product (MODSCAG)[28]. We analysed the difference between the regional snowmelt onset day and the detection dates of the 45 reported overwintering fires, and found that overwintering fires re-emerged on average 27 days (standard deviation, 18.5 days) after the regional snowmelt onset. Regionally, overwintering fires on average re-emerged at the end of May (Julian day 150; standard deviation, 17.9 days). We therefore used the 90th percentile of 48 days after the regional snowmelt onset as the temporal threshold within the detection algorithm for overwintering fires. Because the satellite product detects fires on average two days later than fire managers, we increased the temporal threshold to a total of 50 days. Lastly, in addition to the spatial and temporal constraints, our algorithm eliminated fires that started close to human infrastructure or close in space and time to a recorded lightning strike (Extended Data Fig. 4). Excluding

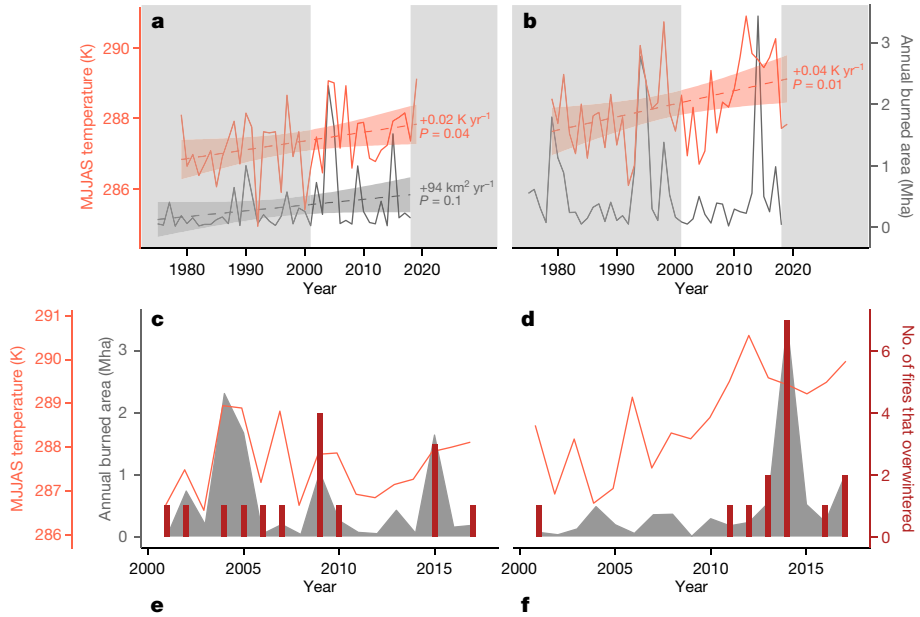

e

Alaska	MJJAS temperature	Burned area	Overwintering fires
MJJAS temperature		$P < 0.001$	$P = 0.03$
Burned area	$\rho = 0.59$		$P = 0.046$
Overwintering fires	$\rho = 0.54$	$\rho = 0.49$	

f

Northwest Territories	MJJAS temperature	Burned area	Overwintering fires
MJJAS temperature		$P < 0.01$	$P < 0.001$
Burned area	$\rho = 0.41$		$P = 0.08$
Overwintering fires	$\rho = 0.77$	$\rho = 0.44$	

Fig. 2 | Temporal drivers of overwintering fires and their long-term trends. Left column, data from Alaska; right column, data from the Northwest Territories. **a**, **b**, Plots of daily maximum temperature for May–September ('MJJAS temperature'; orange) and annual burned area (black). Annual burned area is correlated with MJJAS temperature for Alaska (**a**, Spearman's $\rho = 0.59$, $P < 0.001$) and the Northwest Territories (**b**, $\rho = 0.41$, $P < 0.01$), and is increasing in Alaska ($P = 0.10$). MJJAS temperature is increasing in Alaska ($P = 0.04$) and the Northwest Territories ($P = 0.01$). **c**, **d**, Plots of annual burned area (grey shading), MJJAS temperature (orange lines) and number of fires that overwintered following that year (red columns). Overwintering fires are plotted in their year of origin (the year of onset of overwintering) rather than their year of re-emergence. **e**, **f**, Tabular representations of correlations. The number of large overwintering fires correlates with burned area from the previous year in Alaska (**c**, **e**, $\rho = 0.49$, $P = 0.05$) and the Northwest Territories (**d**, **f**, $\rho = 0.44$, $P = 0.08$), and with MJJAS temperature of the previous year in Alaska (**e**, $\rho = 0.54$, $P = 0.03$) and the Northwest Territories (**f**, $\rho = 0.77$, $P < 0.001$). Large overwintering fires include flare-ups from official reports and additional fires identified by our algorithm. Dashed lines represent trends, shaded areas their 95% confidence interval. White areas in **a** and **b** refer to the period from 2001 to 2018. Extended Data Fig. 6 offers scatterplots of all correlations for visual inspection.

areas close to infrastructure means some overwintering fires may be missed, but eliminates a larger number of false positives from spring pile burning and other anthropogenic influences around settlements.

In addition to the 45 small reported overwintering fires, which we used for algorithm development, we used a subset of nine larger overwintering fires (mean size, 20,312 ha; standard deviation, 24,185 ha), which were large enough to be detected by the MODIS active fire product, as validation data for our algorithm (Supplementary Table 1). We extracted the re-emergence date and distance to burn scars of the previous year for all ignitions from the Alaskan Fire Emissions Database (AKFED)[29], and applied our detection algorithm to them. We detected seven out of nine of the large field-verified overwintering fires.

Furthermore, we identified 20 previously unreported large overwintering fires in Alaska and the Northwest Territories between 2002 and 2018 (Supplementary Table 2). Large overwintering fires constitute 0.8% of the total burned area and 0.5% of the total carbon emissions, yet their relative contribution can be substantial in individual years and amounted to more than 5% in three years in Alaska (2007, 2008 and 2010) and two years in the Northwest Territories (2002 and 2015). For example, in Alaska in 2008, the contribution of a single overwintering fire that burned 13,700 ha amounted to 38% of the annual burned area.

Temporal drivers of overwintering fires

Years with large annual burned area more frequently produced overwintering fires (Fig. 2). Fire season temperature and annual burned area were strongly correlated for both interior Alaska (Spearman's $\rho = 0.59$, $P < 0.001$) and the Northwest Territories ($\rho = 0.41$, $P = 0.097$), and we found increasing temperature trends in both areas, and in burned area for interior Alaska (Fig. 2). Temperature trends differed within regions, and the largest warming was observed in western interior Alaska and central Northwest Territories (Extended Data Fig. 5). Fire season temperature and burned area correlated strongly with the number of overwintering fires in both regions (Fig. 2, Extended Data Fig. 6). Several fires of the large fire years 2009 and 2015 in Alaska and the extreme 2014 fire season in the Northwest Territories overwintered. While burned area in the preceding year is a prerequisite for the occurrence of overwintering fires, we found that fires survived winter following the six hottest summers in the Northwest Territories; in contrast, overwintering was not observed after the seven coolest summers. Our results based on average fire season temperature are further supported by an analysis that focused on extreme temperatures (Extended Data Fig. 7). We found that the number of hot days that surpassed the longer-term 90th percentile of daily maximum temperature during the fire season correlated strongly with annual burned area (Alaska: $\rho = 0.71$, $P < 0.001$; Northwest Territories: $\rho = 0.50$, $P = 0.001$), and with the number of fires that overwintered. Large-scale climatic drivers thus govern the survival and growth of overwintering fires. In autumn, fires in boreal regions are usually extinguished by substantial rain events[1]. Extended fire seasons and droughts associated with climate warming[30,31] may counteract the natural fire extinction in autumn and instead increase the chances of fires entering a smouldering phase. An important driver modulating

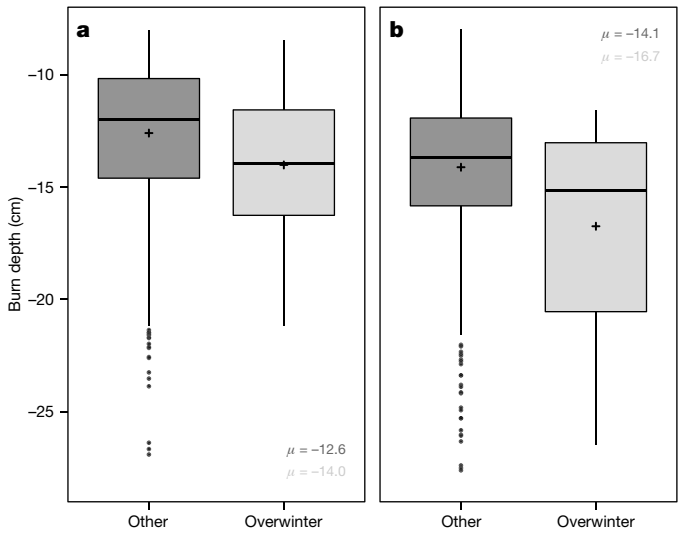

Fig. 3 | Burn depth and overwintering. Burn scars that generate overwintering fires (light grey, 'Overwinter') had burned deeper into the soil organic layer than burn scars that did not generate overwintering fires (dark grey, 'Other') in Alaska (**a**, $P = 0.07$) and the Northwest Territories (**b**, $P = 0.02$). Horizontal lines represent the median, plus (+) signs the mean, μ, and lower and upper ends of each box the 25th and 75th percentiles. Whiskers extend up to 1.5 times the interquartile range, sample points beyond that are represented as dots. We included overwintering fires from government reports and our algorithm.

the emergence of large overwintering fires may therefore be warm and extreme summers that facilitate long and large fire seasons[31,32]. Within our time series, we found no evidence that winter and spring meteorology or snowmelt timing influence the survival of large overwintering fires (Extended Data Tables 1, 2).

Our reference data on overwintering fires contained five times as many small fires (undetected by satellite imagery) as large, detected fires. This suggests that small fires, when re-emerging in spring, usually remain relatively small and undetected, and only occasionally grow large when fire weather conditions favour fire spread. Large overwintering fires on average experienced more severe fire weather at the time of the flare-up than small overwintering fires (Extended Data Table 3), yet this relationship may partly be confounded by interacting effects of fire spread direction and limited fuel availability in the burned area of the preceding year.

Spatial drivers of overwintering fires

For a fire to overwinter, it needs to burn deep into the organic soil or underneath tree roots so that the organic soil can protect and insulate it from adverse winter conditions[33]. Severe fires burn deep into the soil organic layers[34] and may thus help to sustain the smouldering phase of overwintering fires during winter. We analysed burn depth data from AKFED, and found that, on average, fires that promoted overwintering had burned deeper into the organic soil layer than those that stopped burning at the end of the fire season for both Alaska (14.0 cm versus 12.6 cm, $P = 0.07$) and the Northwest Territories (16.7 cm versus 14.1 cm, $P = 0.02$) (Fig. 3, Table 1), indicating that deep burning may facilitate overwintering of fires. Regionally, burn depth is correlated with the 90th percentile of daily maximum temperate in summer in both regions (Extended Data Fig. 7; Alaska: $\rho = 0.56$, $P = 0.02$, Northwest Territories: $\rho = 0.48$, $P = 0.047$). Extreme temperatures have increased since 1979 in western interior Alaska and central and southern Northwest Territories (Extended Data Fig. 5).

Burn depth in organic layers is co-influenced by fire weather, topographic landscape position, and vegetation and soil characteristics[11,12,35,36]. We compared topographic indicators, pre-fire tree cover, tree species dominance and carbon in the organic soil layer of fires that produced overwintering fires to those in fires that did not facilitate overwintering (Table 1). Overwintering fires were associated with flat, low-elevation areas, both in Alaska and the Northwest Territories (Fig. 4, Table 1). Lowland terrain in Alaska and the Northwest Territories typically features thick organic soil. Indeed, overwintering fires occur more often in areas with higher carbon contents in the upper soil layer (0–30 cm) in Alaska ($P = 0.003$), however, this driver was not significant in the Northwest Territories ($P = 0.42$). Tree cover and species modulate fire severity by their influence on fuel availability and connectivity[37]. We found that fires that produced overwintering fires have a higher tree cover ($P = 0.001$) and a larger fraction of black spruce ($P = 0.09$) in Alaska, yet these drivers were not significant in the Northwest Territories ($P = 0.87$ and $P = 0.34$, respectively). Fires occur in more varied landscapes with regard to soil carbon content and forest composition in Alaska compared to the Northwest Territories (Table 1), which may explain why some of these drivers were significant in Alaska but not in the Northwest Territories.

Table 1 | Influence of spatial variables on overwintering

Region	Variable	Source	$\mu_{overwinter}$ (±s.d.)	μ_{other} (±s.d.)	*P*
Alaska	Burn depth	Alaska Fire Emissions Database v3	14.0 (±3.6) cm	12.6 (±3.3) cm	**0.067**
NWT			16.7 (±4.4) cm	14.1 (±3.3) cm	**0.019**
Alaska	Elevation	ArcticDEM	214.5 (±149.5) m	402.7 (±358.7) m	**<0.001**
NWT			270.5 (±95.4) m	356.9 (±224.0) m	**0.001**
Alaska	Slope	ArcticDEM	2.51° (±2.94°)	6.71° (±6.95°)	**<0.001**
NWT			1.86° (±1.20°)	2.90° (±4.08°)	**0.001**
Alaska	Fraction tree cover	MODIS vegetation continuous fields product (MOD44B)	0.37 (±0.16)	0.27 (±0.17)	**0.001**
NWT			0.23 (±0.09)	0.24 (±0.12)	0.87
Alaska	Fraction black spruce	Fuel Characteristic Classification System	0.35 (±0.25)	0.25 (±0.23)	**0.09**
NWT		Beaudoin et al.[43]	0.28 (±0.17)	0.23 (±0.16)	0.34
Alaska	Organic carbon content in upper (0–30 cm) soil layer	Northern Circumpolar Soil Carbon Database	14.87 (±7.4) kg m^{-2}	9.5 (±5.1)	**0.003**
NWT			8.3 (±5.0) kg m^{-2}	9.3 (±6.1)	0.42

NWT, Northwest Territories. Spatial variables differ for fires that produced overwintering fires ('$\mu_{overwinter}$') compared to fires that did not ('μ_{other}'). *P* values are based on Welch *t*-test. Analysis is based on all (small and large, reported and newly identified) overwintering fires. References for data sources are given in the Methods. Bold font in the rightmost column refers to *P* values smaller than 0.1.

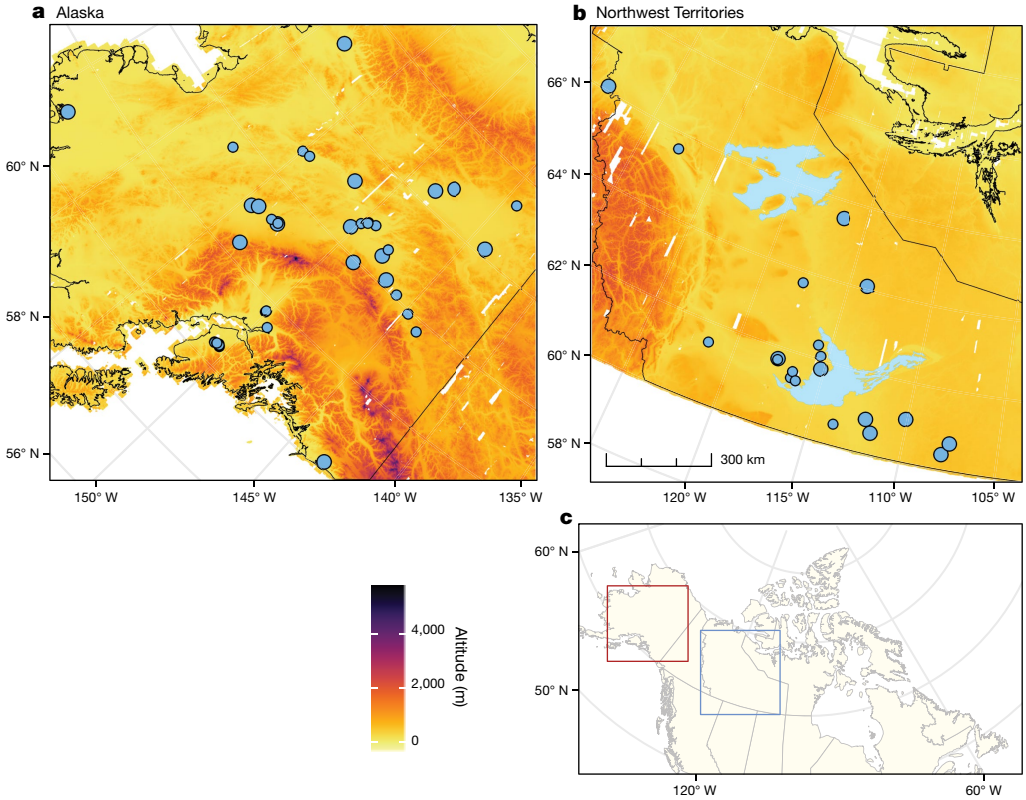

Fig. 4 | Occurrence of overwintering flare-ups. Overwintering flare-ups (blue dots) predominantly occur in lowland areas of Alaska (**a**) and the Northwest Territories (**b**). Small dots, small overwintering fires that were not detected by the Moderate Resolution Imaging Spectroradiometer (MODIS) active fire products; large dots, large fires reported and identified by our algorithm. White areas represent data gaps in the ArcticDEM. Maps were plotted in R. **c**, Location of maps shown in **a** and **b**. Base maps made with Natural Earth.

Climate change and fire management

We identified three main drivers of overwintering fires that are influenced directly by climate warming: summer temperature extremes, large annual fire extent and deep burning. Higher temperatures in boreal regions lead to intensified drought and elongated fire seasons[32]. Longer fire seasons allow fires to spread faster and grow larger, thereby leading to large area burned[38]. Summer heat and drought induce deep drying of surface organic fuels, and are thus associated with higher fire severity and deep burning[12]. Increasing summer temperatures associated with climate warming may thus promote the survival of overwintering fires in the future. Likewise, earlier onset of spring fire weather conditions may lead to a larger fraction of these fires growing large. At the same time, ecosystem shifts towards a dominance of deciduous vegetation due to increasing fire severity[39] and higher temperatures[40] may constrain the occurrence of overwintering fires in the future. Hence, the fate of overwintering fires in the changing boreal biome will depend on counteracting processes that facilitate or constrain their occurrence.

Overwintering fires are currently a relatively rare phenomenon in boreal forests. Yet, because of their long duration and extended smouldering phase, overwintering fires may substantially influence soil functioning and post-fire recovery trajectories[34]. We estimated that large overwintering fires in Alaska and the Northwest Territories emitted 3.5 (standard deviation, 1.1) Tg of carbon between 2002 and 2018, 64% of which occurred during the 2015 Northwest Territories and 2010 Alaska fire seasons. The contribution of smouldering combustion is generally underestimated in carbon emission estimates from boreal fires[20]. Thus, our estimate is likely to be conservative, because overwintering fires exhibit a substantial smouldering phase and may burn deeper than our emissions model currently predicts. In addition, smouldering fires emit relatively more methane and less carbon dioxide in comparison to flaming fires[41], yet methane has a much larger global warming potential[42].

Carbon emissions from overwintering fires currently contribute 0.5% of the total carbon emissions from fires in Alaska and the Northwest Territories, yet this fraction may grow larger with climate warming. We have shown that overwintering fires have temporal and spatial predictability. Space- and air-borne monitoring of the edges of burn scars from the preceding year in lowland forested peatlands early in the fire season, and especially after a year with large burned area, may prove beneficial for detecting and suppressing flare-ups from overwintering fires while they are small. Fire suppression has shown to be most successful and cost-effective when applied early and on small fires[16,17]. Out of the 26 overwintering fires for which we had suppression cost data in Alaska, the single largest fire caused 80% ($2.2 million) of the total costs incurred by all overwintering fires (Supplementary Tables 1 and 2). Early detection and attack on overwintering fires could thus contribute to savings in the fire management budget that is under increasing pressure[18]. In addition, targeted monitoring and early suppression of overwintering fires could help fire managers to preserve terrestrial carbon stores when suppression is part of a climate change mitigation strategy.

Online content

Any methods, additional references, Nature Research reporting summaries, source data, extended data, supplementary information, acknowledgements, peer review information; details of author contributions and competing interests; and statements of data and code availability are available at https://doi.org/10.1038/s41586-021-03437-y.

1. Sedano, F. & Randerson, J. T. Multi-scale influence of vapor pressure deficit on fire ignition and spread in boreal forest ecosystems. *Biogeosciences* **11**, 3739–3755 (2014).
2. Veraverbeke, S. et al. Lightning as a major driver of recent large fire years in North American boreal forests. *Nat. Clim. Chang.* **7**, 529–534 (2017).
3. Calef, M. P., McGuire, A. D. & Chapin, F. S. Human influences on wildfire in Alaska from 1988 through 2005: an analysis of the spatial patterns of human impacts. *Earth Interact.* **12**, 1–17 (2008).
4. McCarty, J. L., Smith, T. E. L. & Turetsky, M. R. Arctic fires re-emerging. *Nat. Geosci.* **13**, 658–660 (2020).
5. Irannezhad, M., Liu, J., Ahmadi, B. & Chen, D. The dangers of Arctic zombie wildfires. *Science* **369**, 1171 (2020).
6. Rein, G. in *Fire Phenomena and the Earth System: An Interdisciplinary Guide to Fire Science* (ed. Belcher, C. M.) 15–34 (Wiley-Blackwell, 2013).
7. Post, E. et al. The polar regions in a 2°C warmer world. *Sci. Adv.* **5**, eaaw9883 (2019).
8. Overland, J. E., Wang, M., Walsh, J. E. & Stroeve, J. C. Future Arctic climate changes: adaptation and mitigation time scales. *Earth's Future* **2**, 68–74 (2014).
9. Tarnocai, C. et al. Soil organic carbon pools in the northern circumpolar permafrost region. *Glob. Biogeochem. Cycles* **23**, GB2023 (2009).
10. Walker, X. J. et al. Increasing wildfires threaten historic carbon sink of boreal forest soils. *Nature* **572**, 520–523 (2019).
11. Turetsky, M. R. et al. Recent acceleration of biomass burning and carbon losses in Alaskan forests and peatlands. *Nat. Geosci.* **4**, 27–31 (2011).
12. Walker, X. J. et al. Soil organic layer combustion in boreal black spruce and jack pine stands of the Northwest Territories, Canada. *Int. J. Wildl. Fire* **27**, 125–134 (2018).
13. Turetsky, M. R. et al. Global vulnerability of peatlands to fire and carbon loss. *Nat. Geosci.* **8**, 11–14 (2015).
14. Flannigan, M. D. et al. Fuel moisture sensitivity to temperature and precipitation: climate change implications. *Clim. Change* **134**, 59–71 (2016).
15. Coops, N. C., Hermosilla, T., Wulder, M. A., White, J. C. & Bolton, D. K. A thirty year, fine-scale, characterization of area burned in Canadian forests shows evidence of regionally increasing trends in the last decade. *PLoS One* **13**, e0197218 (2018).
16. USDA Forest Service, USFS-USDI and NASF. *Large Fire Cost Reduction Action Plan* https://www.fs.usda.gov/sites/default/files/media_wysiwyg/5100_largefirecostreductionaction_mar_03.pdf (2003).
17. Podur, J. & Wotton, M. Will climate change overwhelm fire management capacity? *Ecol. Modell.* **221**, 1301–1309 (2010).
18. Tymstra, C., Stocks, B. J., Cai, X. & Flannigan, M. D. Wildfire management in Canada: review, challenges and opportunities. *Prog. Disaster Sci.* **5**, 100045 (2020); erratum **8**, 100045 (2020).
19. Stocks, B. J. et al. Large forest fires in Canada, 1959–1997. *J. Geophys. Res.* **107**, https://doi.org/10.1029/2001JD000484 (2002).
20. Wiggins, E. B. et al. Evidence for a larger contribution of smoldering combustion to boreal forest fire emissions from tower observations in Alaska. *Atmos. Chem. Phys.* https://doi.org/10.5194/acp-2019-1067 (in the press).
21. Rein, G., Garcia, J., Simeoni, A., Tihay, V. & Ferrat, L. Smouldering natural fires: comparison of burning dynamics in boreal peat and Mediterranean humus. *WIT Trans. Ecol. Environ.* **119**, 183–192 (2008).
22. Baber, C. & McMaster, R. 2019 Alaska Statewide Annual Operating Plan. https://fire.ak.blm.gov/administration/asma.php (Alaska Statewide Master Agreement, 2019).
23. Alaska Interagency Coordination Center. 2010 Alaska fire statistics. https://www.frames.gov/catalog/12055 (Wildland Fire Summary and Statistics Annual Report, 2010).
24. Alaska Division of Forestry. State Forestry monitoring hot spots that overwintered from Deshka Landing Fire. https://akfireinfo.com/2020/04/10/state-forestry-monitoring-hot-spots-that-overwintered-from-deshka-landing-fire/ (2020).
25. Giglio, L., Schroeder, W. & Justice, C. O. The collection 6 MODIS active fire detection algorithm and fire products. *Remote Sens. Environ.* **178**, 31–41 (2016).
26. Kasischke, E. S., Rupp, T. S. & Verbyla, D. L. in *Alaska's Changing Boreal Forest* (eds Chapin, F. S. III, Oswood, M. et al.) 285–301 (Oxford Univ. Press, 2006).
27. Westerling, A. L., Hidalgo, H. G., Cayan, D. R. & Swetnam, T. W. Warming and earlier spring increase western U.S. forest wildfire activity. *Science* **313**, 940–943 (2006).
28. Painter, T. H. et al. Retrieval of subpixel snow covered area, grain size, and albedo from MODIS. *Remote Sens. Environ.* **113**, 868–879 (2009).
29. Scholten, R. C., Jandt, R. R., Miller, E. A., Rogers, B. M. & Veraverbeke, S. ABoVE: Ignitions, burned area and emissions of fires in AK, YT, and NWT, 2001–2018. https://doi.org/10.3334/ORNLDAAC/1812 (2020).
30. Xiao, J. & Zhuang, Q. Drought effects on large fire activity in Canadian and Alaskan forests. *Environ. Res. Lett.* **2**, 044003 (2007).
31. Flannigan, M. D. et al. Global wildland fire season severity in the 21st century. *For. Ecol. Manage.* **294**, 54–61 (2013).
32. Jolly, W. M. et al. Climate-induced variations in global wildfire danger from 1979 to 2013. *Nat. Commun.* **6**, 7537 (2015).
33. Adams, W. H. *The Role of Fire in the Alaska Taiga. An Unsolved Problem* (Bureau of Land Management, State Office, Anchorage, AK, 1974); preprint at https://scholarworks.alaska.edu/handle/11122/6675 (2016).
34. Certini, G. Effects of fire on properties of forest soils: a review. *Oecologia* **143**, 1–10 (2005).
35. Kane, E. S., Kasischke, E. S., Valentine, D. W., Turetsky, M. R. & McGuire, A. D. Topographic influences on wildfire consumption of soil organic carbon in interior Alaska: implications for black carbon accumulation. *J. Geophys. Res. Biogeosci.* **112**, 1–11 (2007).
36. Hoy, E. E., Turetsky, M. R. & Kasischke, E. S. More frequent burning increases vulnerability of Alaskan boreal black spruce forests. *Environ. Res. Lett.* **11**, 095001 (2016).
37. Miyanishi, K. & Johnson, E. A. Process and patterns of duff consumption in the mixedwood boreal forest. *Can. J. For. Res.* **32**, 1285–1295 (2002).
38. Kasischke, E. S. & Turetsky, M. R. Recent changes in the fire regime across the North American boreal region — spatial and temporal patterns of burning across Canada and Alaska. *Geophys. Res. Lett.* **33**, https://doi.org/10.1029/2006GL025677 (2006).
39. Johnstone, J. F. et al. Factors shaping alternate successional trajectories in burned black spruce forests of Alaska. *Ecosphere* **11**, https://doi.org/10.1002/ecs2.3129 (2020).
40. Mekonnen, Z. A., Riley, W. J., Randerson, J. T., Grant, R. F. & Rogers, B. M. Expansion of high-latitude deciduous forests driven by interactions between climate warming and fire. *Nat. Plants* **5**, 952–958 (2019).
41. Andreae, M. O. & Merlet, P. Emission of trace gases and aerosols from biomass burning. *Glob. Biogeochem. Cycles* **15**, 955–966 (2001).
42. Dean, J. F. et al. Methane feedbacks to the global climate system in a warmer world. *Rev. Geophys.* **56**, 207–250 (2018).
43. Beaudoin, A., Bernier, P. Y., Villemaire, P., Guindon, L. & Guo, X. J. Tracking forest attributes across Canada between 2001 and 2011 using a k nearest neighbors mapping approach applied to MODIS imagery. *Can. J. For. Res.* **48**, 85–93 (2018).

Methods

Verified overwintering fires

Fire managers in Alaska and Canada routinely document information on all fires detected in their territory. These data are assembled in the Alaska Wildland Fire Maps (AWFP; https://fire.ak.blm.gov/predsvcs/maps.php) and the Canadian National Fire Database (CNFD)[19]. These databases contain the discovery date and location of fires as well as numerous fire attributes, such as the size, end date, estimated costs and fire cause. Fire managers attribute ignition causes based on expert knowledge, ground truth or helicopter data, and other sources such as satellite imagery and lightning data. Causes in the fire databases only include human and lightning sources. With rising awareness of overwintering fires, however, some fire managers sparsely started documenting these re-emerging fires in a separate database. We assembled the timing and location of re-emergence of 54 overwintering fires, 42 in Alaska, USA, and 12 in the Northwest Territories, Canada, from these fire management reports. The key characteristics of the overwintering fires used in our study can be found in Supplementary Table 1. Cost data for the fires in Supplementary Tables 1 and 2 were taken from interagency Incident Status Summaries (209 reports) and provided by the Bureau of Land Management, where available, and supplemented by the estimated costs listed in the AWFP database.

Fire data

We derived the burned area and day of burning for Alaska and the Northwest Territories between 2001 to 2018 at 500-m spatial resolution using the Alaskan Fire Emissions Database (AKFED) version 3[29], which was updated with input from the Moderate Resolution Imaging Spectroradiometer (MODIS) Collection 6[2,25]. Daily burned area was retrieved by combining fire perimeter data from the AWFP and the CNFD, and remotely sensed surface reflectance and active fire data from MODIS. After integration of MODIS Collection 6, total burned area and carbon emissions remained within 5% of previous estimates[2,44].

The location of the first day of burning of a fire marks the ignition point. We therefore extracted the location and timing of ignitions from local minima within the day of burning variable, denoting the earliest burn date, within each fire perimeter. Fires originating from multiple separate ignitions sometimes grow together in a multi-ignition fire complex. Our algorithm therefore allowed for several ignition points per fire perimeter by using a local minimum search radius of 5 km. Although MODIS provides daily coverage of active fires and burned area, the actual ignition location can be obscured if clouds are present, or if a fire starts several hours before the satellite overpass and spreads fast. In these cases, the local minimum contained multiple pixels with the same day of burning. When multiple neighbouring pixels burned at the same day, we estimated the ignition location as the centroid of these pixels and calculated the spatial uncertainty of the ignition locations from the standard deviation in the x and y coordinates of these burned pixels. The spatial standard deviation of the ignition location is a measure of the ignition location uncertainty. Since the native resolution of the MODIS active fire data is 926.6 m, we added a buffer of 1 km to all ignition locations. For fires with multiple burned pixels on the start date, we extended this 1-km buffer with the spatial standard deviation of the ignition location.

Burn depth and emissions were also derived from AKFED version 3, which predicts carbon consumption and burn depth based on remotely sensed pre-fire tree cover, the differenced normalized burn ratio, and the temperature and drought code at the day of burning using a non-linear multiplicative regression model ($R^2 = 0.39$)[2]. The model was developed using field observations from black spruce (*Picea mariana*) ecosystems. Primary sources of uncertainties that influence the carbon consumption estimate include the unexplained variance in the regression model, the underlying land cover classifications, and consumption scaling for non-black-spruce ecosystems. To eliminate uncertainties from consumption scaling in our spatial analysis, we excluded burn scars with high dominance (more than 90%) of ecosystems other than black spruce. Pixel-level uncertainties in carbon consumption were within 20–25% of the pixel-level predictions[44].

We used fire perimeter data from the CNFD and AWFP to calculate burned area for 1975 to 2000. Since these fire perimeters do not account for unburned islands in the mapped area, we normalized their burned area with AKFED burned area. As in ref. [2], we assumed that uncertainties in fire perimeter mapping have reduced since the integration of Landsat imagery in fire mapping around 1975[45]. The minimum mapping unit (MMU) for the CNFD was 200 ha, and changed over time for AWFP, from 405 ha before 1987 to 40.5 ha between 1987 and 2014, and finally to 4.5 ha starting from 2015. We calculated the ratio of AKFED burned area, which has a MMU of 25 ha, over the ratio of burned area retrieved from the fire perimeters between 2001 and 2018. To remove uncertainties due to the MMU, we calculated separate ratios excluding all perimeters smaller than 405 ha and smaller than 40.5 ha for Alaska, and all fires smaller than 200 ha for the Northwest Territories. We multiplied the burned-area estimates by the according ratio per region and, in the case of Alaska, time frame. For the Northwest Territories the derived ratio was 0.971, and for Alaska they were 0.829 for fires larger than 405 ha, and 0.825 for fires larger than 40.5 ha.

Lightning data and ignition attribution

We acquired data on lightning strikes between 2001 and 2018 detected by the Alaskan Lightning Detection Network (ALDN)[46] and the Canadian Lightning Detection Network (CLDN)[47], which contained information on location and timing of cloud-to-ground lightning strikes. The ALDN was started by the Bureau of Land Management Alaska Fire Service (BLM-AFS) in 1976 and has since gradually increased in detection accuracy, efficiency and coverage. The detection accuracy is highest for interior Alaska and decreases towards the coast. A substantial upgrade to the system in 2000 led to an increased detection accuracy and efficiency of 0.5–2 km and 80–90%, respectively[46]. The replacement of the impact lightning system with a time of arrival system in 2012 resulted in a further 1.5-fold increase in the detection efficiency, and an increased accuracy stemming from the counting of strokes per flash instead of lightning flashes[48].

Lightning data from the CLDN are available since 1998 and provided by Environment and Climate Change Canada. The CLDN was upgraded gradually, with the largest changes in Northern Canada comprising the addition of two sites in northern Yukon in 2003 and sensor upgrades in the Northwest Territories and Yukon in 2008 and 2010[47,49]. For the southern Northwest Territories, where most of the lightning activity takes place, the CLDN detects approximately 80–90% of the lightning flashes with a positional accuracy of 500 m (ref. [50]). At the periphery of the sensor network, the efficiency decreases to about 70% with positional accuracies between 12 km and 22 km. Lightning detection and accuracy decreases to approximately 30% 300 km beyond the sensor network. Towards the northeastern Northwest Territories, accuracy and efficiency markedly decline owing to a lack of sensor sites.

Between 2001 and 2018, the positional accuracies of the ALDN and CLDN vary substantially in time and space. We therefore adapted a conservative estimate of 2 km for the overall accuracy of the sensor networks and buffered all detected lightning strikes in Alaska and the Northwest Territories using this 2-km buffer.

We used a spatial and a temporal constraint to assess if an ignition may have been caused by lightning. Both the ignition locations and the lightning locations contain location uncertainties. For the spatial constraint, we thus overlaid all ignition locations including their spatial uncertainty buffer with the buffered lightning strikes of the same year. Subsequently, we compared the date of the lightning strike with the ignition date. Fires often smoulder for several days after a lightning strike before they are detected, yet the lag time between a lightning strike and ignition detection in boreal forests of North America is not

known. Lag times of two or three days have been inferred for fires in Australia, Finland and Florida, USA[51–53]. We extended the lag time threshold to six days to account for longer holdover times that may occur owing to the prolonged smouldering in organic soils in boreal North America. Thus, we classified fires with a lightning strike up to six days before the ignition date as started by lightning. We also accounted for a temporal uncertainty of one day in ignition timing[54]. We thereby identified 85% of the lightning ignitions as reported in the AWFP and CNFD (Extended Data Fig. 4a).

Infrastructure data

We used vector data on roads and other infrastructure elements to assess if an ignition may have been caused by anthropogenic activity. For Alaska, the Alaska Infrastructure 1:63,360 shapefile (2006) provided by the Department of Natural Resources comprises all roads and trails, and power and electrical lines. The same infrastructure elements are available from various infrastructure data sets of the Northwest Territories, including the 2010 Road Network File by Statistics Canada[55] and the Roads 1M data set by the Government of Yukon[56], which we combined here.

In Alaska, 99% of ignitions up to 5 km from settlements are human-induced[3]. We used all fires classified as human-ignited by the AWFP and CNFD to derive a distance threshold from our data. First, we calculated the distance between each ignition point including its uncertainty buffer and its nearest infrastructure element for all ignition points that fell within a distance of 5 km of an infrastructure element. Then, we derived a statistical distribution of these distances for all fires that were classified as human-ignited in the official fire databases. 75% of the ignitions were within 1 km of an infrastructure element (Extended Data Fig. 4b). We therefore classified fires that fell within 1 km of an infrastructure element as human-ignited.

Snow cover data

We determined the regional first snow-free day of spring between 2001 and 2018 from the MODIS daily fractional snow cover product (MODSCAG)[28]. MODSCAG computes the snow fraction of each 500-m pixel using spectral mixture analysis and has been shown to outperform normalized difference snow-index-based methods, especially during periods of accumulation and melt[57]. We flagged a pixel as snow-free when its fractional snow cover dropped below 15%. We determined the period between 21 March (Julian day 80) and 1 July (Julian day 182) as spring season, and selected the first snow-free day of each pixel during this period. Pixels that were still snow-covered by 1 July were flagged as permanent snow cover and excluded from the analysis. We also excluded pixels with persistent missing data due to cloud cover on four or more days preceding the first snow-free day detection. The resulting retrieval contained data for 98% of interior Alaska and 87% of interior Northwest Territories.

For a regional estimate, we calculated the yearly mean of the first snow-free day within the interior boreal regions of Alaska and the Northwest Territories. For Alaska this refers to the intermontane boreal ecoregions between the Brooks Range and the Alaska Range, excluding the coastal Bering ecoregions[58]. For the Northwest Territories we selected the taiga plains and taiga shield ecozones in the Northwest Territories[59]. Only pixels that contained data for all years and had not burned during the 18-year timeframe were included in the regional mean.

Climate and fire weather data

We extracted meteorological data from the North America Regional Reanalysis[60] (NARR) for our climate analysis. NARR provides climate reanalysis data since 1979 at a 32-km resolution based on the NCEP Eta atmospheric model and the Regional Climate Data Assimilation System. We extracted 3-hourly air temperature at 2 m, relative humidity, wind speed and precipitation over Alaska and the Northwest Territories, and calculated monthly means of the 3-h period that included local solar noon. We derived vapour pressure deficit (VPD) and fire weather variables following the Canadian Fire Weather Index System (CFWIS)[61] from meteorological variables.

Detection of large overwintering fires

45 of the ground-truthed overwintering fires (10 from the Northwest Territories and 35 from Alaska, referred to in the following as 'small fires') were too small to be detected from the MODIS active fire product that was used within AKFED[25] (Supplementary Table 1). We used the spatial and temporal characteristics of these 45 small fires to derive spatial and temporal thresholds for a detection algorithm for larger overwintering fires that can be detected from MODIS imagery. The nine remaining overwintering fires from the fire management reports were large enough to be detected by MODIS and were used as reference data for validation of the detection algorithm (Extended Data Fig. 2).

Overwintering fires re-emerge within or in close proximity to burned area from the year before and earlier in the year than the majority of lightning- and human-ignited fires. We calculated the shortest distance between each of the 45 small overwintering fire locations reported by fire managers and any area burned in the previous year based on our burned-area product and derived a threshold of 1 km based on the statistical distribution of these distances (Extended Data Fig. 3) and the spatial resolution of our satellite product. Distributions of the difference between the detection date of the small overwintering fires and the regional snow melt served as a temporal threshold. We chose a threshold of 48 days, which comprises the 90% quantile of the distribution. On average, fires are detected by our satellite product within 1.7 days of the discovery date of the fire agencies. We therefore extended the threshold by two days to account for the differences in data sources. We applied both thresholds to all ignitions detected by MODIS between 2002 and 2018 to identify potential overwintering fires. From these, we further excluded ignitions that were likely to have been caused by lightning by filtering out all ignitions in the spatiotemporal vicinity of a lightning strike. We intersected ignitions and lightning strikes including their spatial uncertainties (2 km for all lightning strikes and the individual positional inaccuracy of each ignition) and allowed for a lag time of six days between lightning strikes and ignition in combination with an uncertainty of one day in the ignition timing. We also excluded ignitions with a likely human origin when these occurred with 1 km of infrastructure, thereby accounting for the spatial uncertainty of the ignitions' location.

Uncertainty of our algorithm

Our estimate of the number of overwintering fires based on these four constraints and moderate resolution satellite data is likely to be conservative. For the Northwest Territories, for example, some estimates suggest that about one-third of all fires in 2015 were caused by overwintering flare-ups[62]. Our algorithm however only classified 4% of the ignitions to be overwintering fires, although 17.5% of the ignitions were within a 1-km distance from a previous year fire. Many of these ignitions occurred close to a human infrastructure element or late in the season and were therefore removed by our algorithm to avoid false positives. However, our reference data on overwintering fires suggest that 35% of the small fires are indeed found within our infrastructure buffer, and emergence dates as late as July have been reported by fire managers.

Furthermore, many overwintering fires occur in unburned islands or stay relatively small and are therefore not detected by the MODIS active fire product. The Visible Infrared Imaging Radiometer Suite (VIIRS) active fire detection data product[63] has a higher spatial resolution of 375 m and is therefore capable of detecting smaller fires. Indeed, using VIIRS data we could detect a further 8 of the 31 overwintering fires that were too small to be detected by MODIS. However, VIIRS data are only available from 2012 onward, which renders it less useful than MODIS for the analysis of longer time periods.

Spatial drivers of overwintering fires

We extracted burn depth from AKFED for all burn scars. We excluded burn scars with high dominance (more than 90%) of white spruce, pine and deciduous ecosystems because the burn-depth model was developed for black spruce ecosystems. We tested the statistical difference in mean burn depth between burn scars that produced overwintering fires and those that did not using Welch's *t*-test[64,65]. We thereby assumed that overwintering fires were caused by the closest fire of the previous year.

A variety of data sets were used to analyse additional spatial drivers. The analysis was carried out analogously to the burn-depth analysis by comparing the mean over the entire burn scar between fires that produced overwintering fires and those that did not using Welch's *t*-test. We extracted the elevation and slope for all burn scars from the 100-m resolution ArcticDEM v3.0 (refs. [66,67]). ArcticDEM provides high-resolution (up to 2 m) digital surface models of the Arctic from 0.32-m to 0.5-m resolution panchromatic satellite imagery of the DigitalGlobe collection including WorldView-1 (2007), WorldView-2 (2009), WorldView-3 (2014) and GeoEye-1 (2008)[68]. Annual Terra MODIS Vegetation Continuous Fields Collection 6 data at 250-m resolution (MOD44B)[69] for the years 2000–17 were used to derive pre-fire tree cover for each burn scar. Tree species fractions were taken from the Fuel Characteristic Classification System layer of the year 2001[70–72] for Alaska, and from refs. [43,73] for the Northwest Territories. We aggregated the tree species into black spruce (*Picea mariana*), white spruce (*Picea glauca*), deciduous, tundra-grass-shrub and non-vegetated ecosystems, and pine (only present in the Northwest Territories) as described in ref. [2]. Organic carbon content in the upper organic soil layer (0–30 cm depth) was extracted from the Northern Circumpolar Soil Carbon Database[74].

Temporal drivers of overwintering fires

We analysed the relationship between the number of overwintering fires, annual burned area and daily maximum temperatures from NARR on a regional scale. On the basis of scatterplots between all three variables, we chose Spearman correlations because of nonlinearity (Extended Data Fig. 6a, b, e), the presence of outliers (Extended Data Fig. 6d) and small sample sizes (Extended Data Fig. 6c–f, $n = 17$). *P* values were computed for all correlations.

To analyse the influence of winter and spring weather, we computed Spearman's correlations between overwintering fires and the regional snow melt, as well as winter and spring temperature, VPD, precipitation and relative humidity. Analogously to the spatial drivers analyses, we also tested for differences in the snowmelt date and fire weather variables in spring between fire scars that facilitated overwintering, and those that did not using Welsh's *t*-test. For the fire weather variables, we took the average of the 50 days after the average snow melt of each fire. We further compared VPD and fire weather variables at the day of detection for small and large overwintering fires using Welsh's *t*-test to assess the influence of spring fire weather on the growth of overwintering fires.

Data availability

The location and timing of ignition of the overwintering fires used in this study are given in the Supplementary Information. Daily burned area, emissions and ignitions data for Alaska and the Northwest Territories are archived at the Oak Ridge National Laboratory Distributed Active Archive Center for biogeochemical dynamics (https://doi.org/10.3334/ORNLDAAC/1812). Lightning data are available from the Alaska Interagency Coordination Center (https://fire.ak.blm.gov/predsvcs/maps.php) and from Environment and Climate Change Canada. Infrastructure data are available for Alaska from the Department of Natural Resources (https://catalog.data.gov/dataset/alaska-infrastructure-1-63360), and for the Northwest Territories from Statistics Canada (https://www150.statcan.gc.ca/n1/en/catalogue/92-500-X) and the Government of Yukon (https://hub.arcgis.com/datasets/322b6cf3fa1444c289a1d611a4778ead_42/data). MODSCAG snow fraction data are freely available from the JPL Snow Data Server (http://snow.jpl.nasa.gov/portal/). All climate data used in this study are available from the North America Regional Reanalysis (https://psl.noaa.gov/data/gridded/data.narr.html). All data used for the analysis of spatial drivers are freely available, including the ArcticDEM (https://doi.org/10.7910/DVN/OHHUKH), the Northern Circumpolar Soil Carbon Database v2 (https://doi.org/10.5879/ECDS/00000002) and the Fuel Characteristic Classification System (https://www.landfire.gov/fccs.php).

Code availability

Codes used to analyse the data are available from https://github.com/screbec/Overwintering-fires or https://doi.org/10.5281/zenodo.4549321.

44. Veraverbeke, S., Rogers, B. M. & Randerson, J. T. Daily burned area and carbon emissions from boreal fires in Alaska. *Biogeosci. Discuss*. **12**, 3579–3601 (2015).
45. Kasischke, E. S. et al. Quantifying burned area for North American forests: implications for direct reduction of carbon stocks. *J. Geophys. Res. Biogeosci*. **116**, 1–17 (2011).
46. Farukh, M. A. & Hayasaka, H. Active forest fire occurrences in severe lightning years in Alaska. *J. Nat. Disaster Sci*. **33**, 71–84 (2012).
47. Burrows, W. R. & Kochtubajda, B. A decade of cloud-to-ground lightning in Canada: 1999-2008. Part 1: flash density and occurrence. *Atmos.-Ocean* **48**, 177–194 (2010).
48. Bieniek, P. A. et al. Lightning variability in dynamically downscaled simulations of Alaska's present and future summer climate. *J. Appl. Meteorol. Climatol*. **59**, 1139–1152 (2020).
49. Kochtubajda, B. et al. Exceptional cloud-to-ground lightning during an unusually warm summer in Yukon, Canada. *J. Geophys. Res. Atmos*. **116**, https://doi.org/10.1029/2011JD016080 (2011).
50. Kochtubajda, B., Stewart, R. & Tropea, B. Lightning and weather associated with the extreme 2014 wildfire season in Canada's Northwest Territories. In *Proceedings of the 24th International Lightning Detection Conference* 1–4 (VAISALA, 2016).
51. Dowdy, A. J. & Mills, G. A. Atmospheric and fuel moisture characteristics associated with lightning-attributed fires. *J. Appl. Meteorol. Climatol*. **51**, 2025–2037 (2012).
52. Larjavaara, M., Pennanen, J. & Tuomi, T. J. Lightning that ignites forest fires in Finland. *Agric. For. Meteorol*. **132**, 171–180 (2005).
53. Duncan, B. W., Adrian, F. W. & Stolen, E. D. Isolating the lightning ignition regime from a contemporary background fire regime in east-central Florida, USA. *Can. J. For. Res*. **40**, 286–297 (2010).
54. Veraverbeke, S. et al. Mapping the daily progression of large wildland fires using MODIS active fire data. *Int. J. Wildl. Fire* **23**, 655–667 (2014).
55. Statistics Canada. Road Network File 2010. https://www150.statcan.gc.ca/n1/en/catalogue/92-500-X (2016).
56. Government of Yukon. Corporate Spatial Warehouse. ftp://ftp.geomaticsyukon.ca/GeoYukon/Transportation/Roads_1M/ (2018).
57. Rittger, K., Painter, T. H. & Dozier, J. Assessment of methods for mapping snow cover from MODIS. *Adv. Water Resour*. **51**, 367–380 (2013).
58. Gallant, A. L., Binnian, E. F., Omernik, J. M. & Shasby, M. B. *Ecoregions of Alaska* (Professional Paper 1567, USGS, 1995).
59. Canadian Council on Ecological Areas (CCEA). Canada ecozones. https://ccea-ccae.org/ecozones-downloads/ (2016).
60. Mesinger, F. et al. North American regional reanalysis. *Bull. Am. Meteorol. Soc*. **87**, 343–360 (2006).
61. Van Wagner, C. E. *Development and Structure of the Canadian Fire Weather Index System*. Forestry Technical Report Vol. 35 (Canadian Forestry Service Headquarters, Ottawa, 1987).
62. York, A. D. & Jandt, R. R. *Opportunities to Apply Remote Sensing in Boreal/Arctic Wildfire Management & Science: A Workshop Report* www.frames.gov/catalog/57849 (University of Alaska, Fairbanks, 2019).
63. Schroeder, W., Oliva, P., Giglio, L. & Csiszar, I. A. The New VIIRS 375m active fire detection data product: algorithm description and initial assessment. *Remote Sens. Environ*. **143**, 85–96 (2014).
64. Welch, B. L. The significance of the difference between two means when the population variances are unequal. *Biometrika* **29**, 350–362 (1938).
65. Welch, B. L. The generalization of 'Student's' problem when several different population variances are involved. *Biometrika* **34**, 28–35 (1947).
66. Morin, P. et al. ArcticDEM; a publically available, high resolution elevation model of the Arctic. *Geophys. Res. Abstr*. **18**, EGU2016-8396 (2016).
67. Porter, C. et al. ArcticDEM. https://doi.org/10.7910/DVN/OHHUKH (Harvard Dataverse, 2018).
68. Dai, C., Durand, M., Howat, I. M., Altenau, E. H. & Pavelsky, T. M. Estimating river surface elevation from arcticDEM. *Geophys. Res. Lett*. **45**, 3107–3114 (2018).
69. Hansen, M. C. et al. Global percent tree cover at a spatial resolution of 500 meters: first results of the MODIS vegetation continuous fields algorithm. *Earth Interact*. **7**, 1–15 (2003).
70. Pettinari, M. L. & Chuvieco, E. Generation of a global fuel data set using the fuel characteristic classification system. *Biogeosciences* **13**, 2061–2076 (2016).
71. Ottmar, R. D., Sandberg, D. V., Riccardi, C. L. & Prichard, S. J. An overview of the fuel characteristic classification system — quantifying, classifying, and creating fuelbeds for resource planning. *Can. J. For. Res*. **37**, 2383–2393 (2007).

72. Riccardi, C. L. et al. The fuelbed: a key element of the fuel characteristic classification system. *Can. J. For. Res*. **37**, 2394–2412 (2007).
73. Beaudoin, A., Bernier, P. Y., Villemaire, P., Guindon, L. & Guo, X. *Species Composition, Forest Properties and Land Cover Types Across Canada's Forests at 250m Resolution for 2001 and 2011*. https://doi.org/10.23687/ec9e2659-1c29-4ddb-87a2-6aced147a990 (Natural Resources Canada, Canadian Forest Service, Laurentian Forest Centre, 2017).
74. Hugelius, G. et al. The northern circumpolar soil carbon database: spatially distributed datasets of soil coverage and soil carbon storage in the northern permafrost regions. *Earth Syst. Sci. Data* **5**, 3–13 (2013).

Acknowledgements We would like to thank C. Van Der Horn and G. Branson (Alaska Interagency Coordination Center), and M. Coyle (Forest Management Division, Department of Environment and Natural Resources, Government of the Northwest Territories), for providing ground truth data on overwintering fires. We wish to thank Environment and Climate Change Canada for their generous permission to use Canadian Lightning Detection Network data, and the Bureau of Land Management, Alaska Fire Service, for providing cost information. We thank NASA JPL's Snow Data Center for making their MODSCAG data available. This work was funded by the Netherlands Organization for Scientific Research (NWO) through a Vidi grant (Fires Pushing Trees North) awarded to S.V. B.M.R. acknowledges support from the National Aeronautics and Space Administration (NASA) Arctic-Boreal Vulnerability Experiment (ABoVE; NNX15AU56A).

Author contributions S.V. and R.C.S. designed the research; R.C.S. performed the analysis with input from S.V.; B.M.R. contributed to the interpretation of cost data; R.R.J. and E.A.M. contributed to the interpretation of field data; R.C.S. drafted the manuscript; and all authors participated in manuscript editing.

Competing interests The authors declare no competing interests.

Additional information

Supplementary information The online version contains supplementary material available at https://doi.org/10.1038/s41586-021-03437-y.

Correspondence and requests for materials should be addressed to R.C.S.

Peer review information *Nature* thanks the anonymous reviewers for their contribution to the peer review of this work. Peer reviewer reports are available.

Extended Data Fig. 1 | Aerial view of the Seven Mile Slough fire in Alaska on 9 May 2011. Smouldering hotspots (labelled with 'a') had overwintered and burned in the organic soil layer below the spruces of an unburned island. Green tree crowns of the fallen trees (labelled 'b') in the original unburned island (perimeter approximated in black) suggest that tree roots were damaged by subsurface burning. (Photograph by E.A.M.).

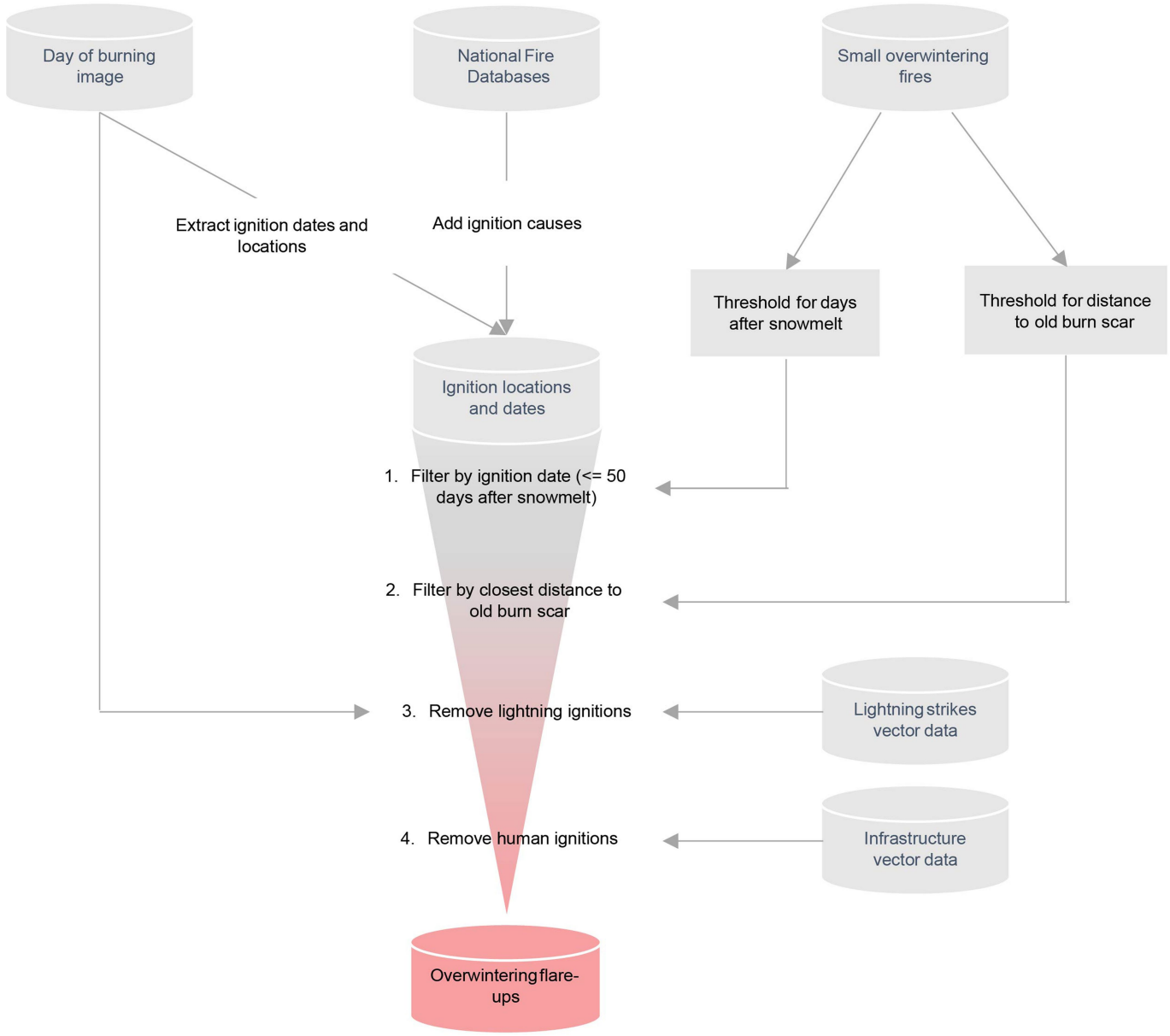

Extended Data Fig. 2 | Workflow used to detect large overwintering fires. First, ignition locations, dates and causes according to official fire databases were extracted. In four steps, the algorithm filters these ignitions by date, distance to an old burn scar, and co-occurrence of lightning strikes and infrastructure elements. Small overwintering fires that were not detected by satellite products were used to derive thresholds for the algorithm.

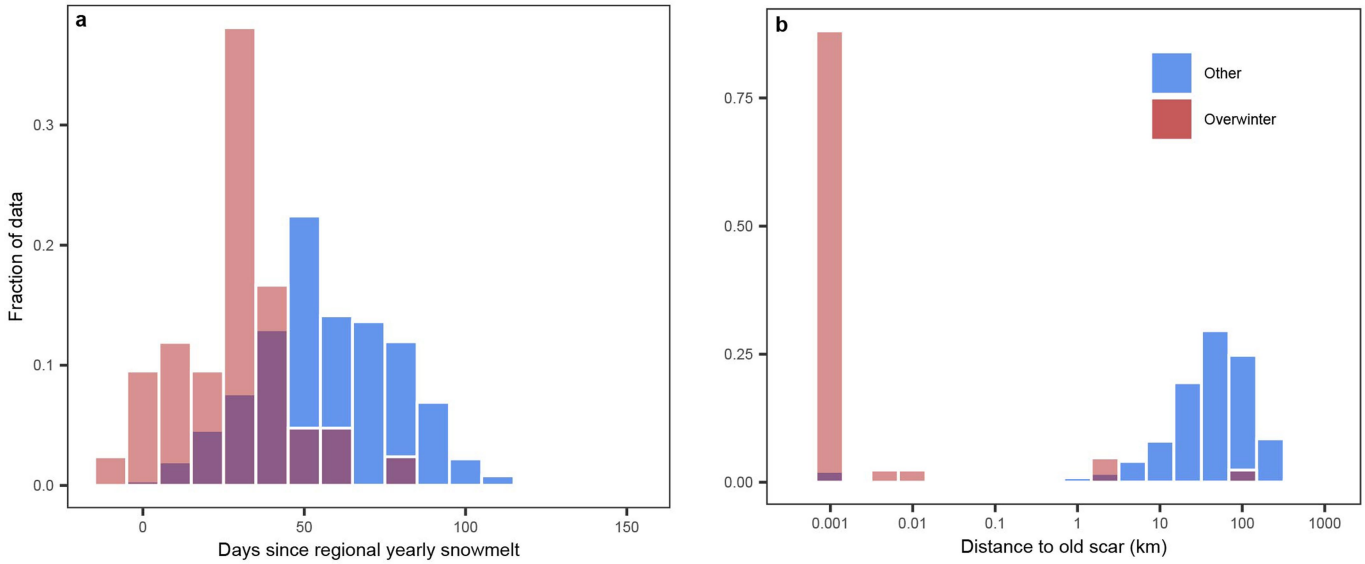

Extended Data Fig. 3 | Spatiotemporal characteristics of small overwintering fires. Overwintering fires emerge earlier after the seasonal snow melt (**a**) and closer to a fire scar from the year before (**b**) than other fires. 'Other fires' refer to all fires not classified as overwintering in official fire databases. Day since regional snow melt was taken from government sources.

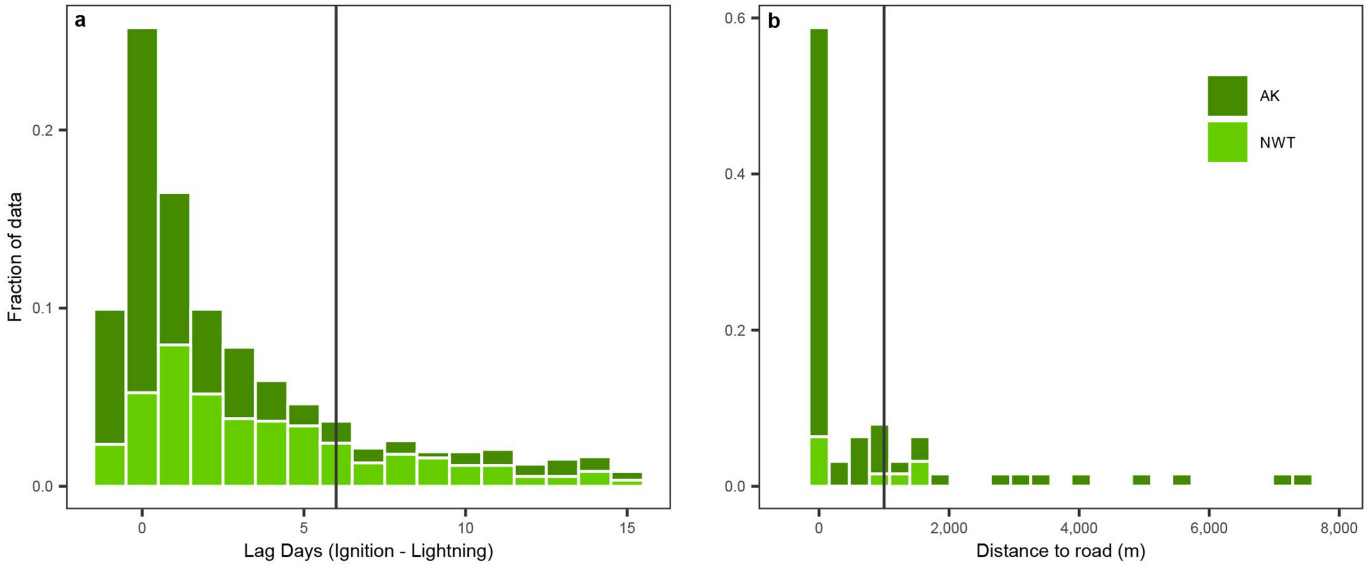

Extended Data Fig. 4 | Lag times and distance to roads. Shown are histograms of lag time between lightning strikes and ignition detections (**a**), and distance to road for ignitions by humans (**b**). Human and lightning ignitions were characterized on the basis of the Alaskan Wildland Fire Maps (Alaska, AK) and the Canadian National Fire Database (Northwest Territories, NWT). The black lines indicate the thresholds used to eliminate potential overwintering fires due to spatial proximity to infrastructure and spatiotemporal proximity to lightning strikes.

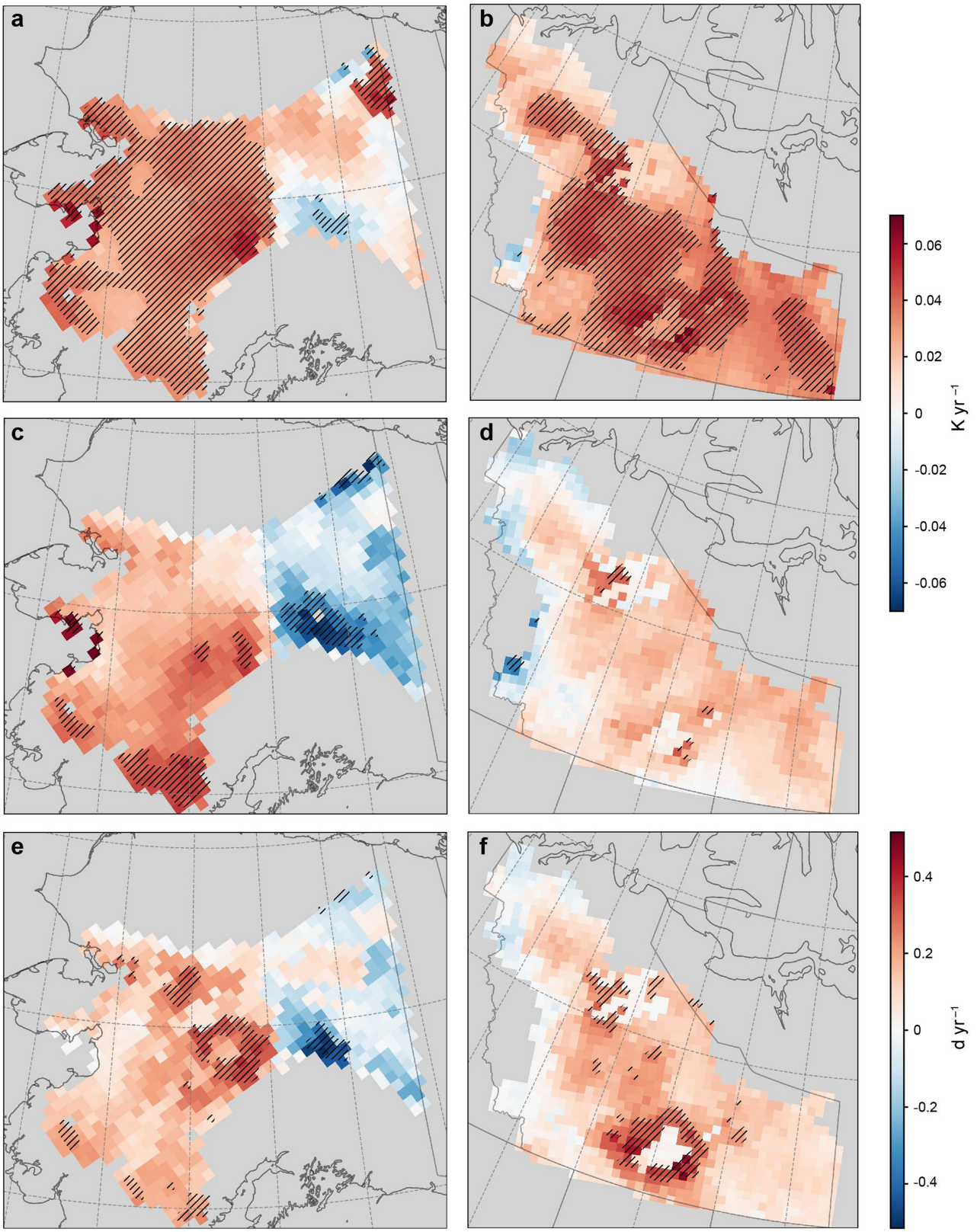

Extended Data Fig. 5 | Average and extreme temperature trends for interior Alaska and the Northwest Territories. a, **b**, Average of the daily maximum temperature of the summer months May–September; **c**, **d**, its 90th percentile. **e**, **f**, Number of hot days surpassing the 90th percentile. Panels **a**, **c**, **e** show data for interior Alaska, and panels **b**, **d**, **f** for the taiga plains and the taiga shield of the Northwest Territories.

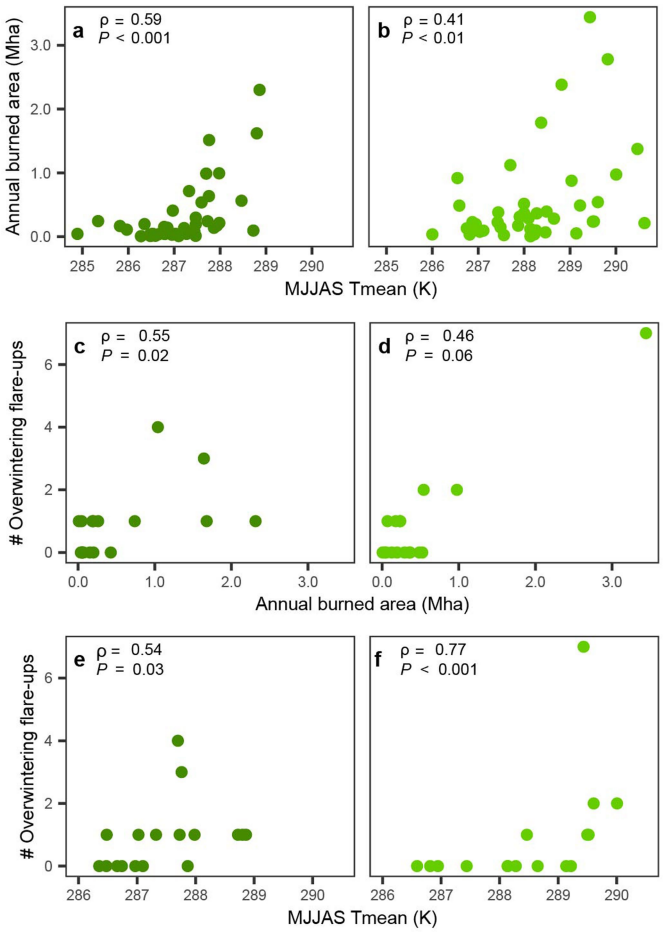

Extended Data Fig. 6 | Scatter plots and Spearman correlations (*ρ*) of summer temperature, burned area and overwintering flare-ups. a, **b**, Daily mean maximum temperature between May and September (MJJAS; T_{mean}) and annual burned area. **c**, **d**, Previous year's burned area and the number of overwintering flare-ups. **e**, **f**, MJJAS maximum temperature and the number of overwintering flare-ups. Panels **a**, **c**, **e** show data for Alaska, and panels **b**, **d**, **f** for the Northwest Territories.

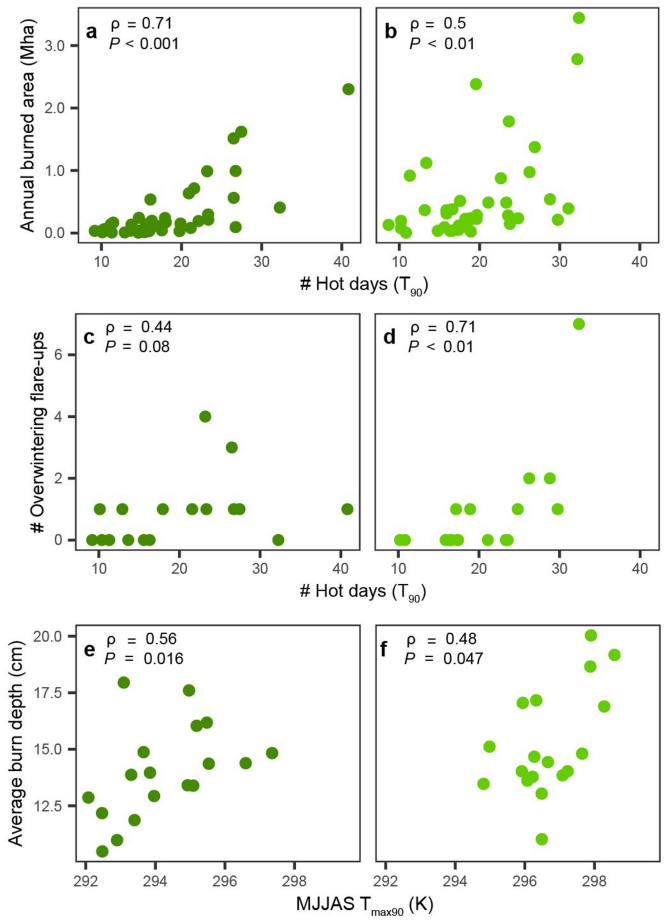

Extended Data Fig. 7 | Scatter plots and Spearman correlations of temperature extremes and burned area, overwintering flare-ups and burn depth. **a**, **b**, Number of MJJAS hot days (days with a maximum temperature hotter than the 1979–2020 90th percentile, T_{90}) and burned area. **c**, **d**, Number of MJJAS hot days and overwintering ignitions. **e**, **f**, 90th percentile of MJJAS temperature (T_{max90}) and average burn depth. Panels **a**, **c**, **e** show data for Alaska, and panels **b**, **d**, **f** for the Northwest Territories.

Extended Data Table 1 | Correlation of meteorology and the number of overwintering flare-ups

Region	Variable	-	Oct	Nov	Dec	Jan	Feb	Mar	Apr	May
Alaska	Regional snow melt	-0.22								
Northwest Territories		-0.06								
Alaska	Average temperature		0.04	0.17	0.05	-0.05	0.16	0.22	0.18	0.08
Northwest Territories			0.37	-0.06	0.08	0.24	0.11	0.29	-0.14	0.22
Alaska	Vapour Pressure Deficit (VPD)		-0.24	-0.07	0.23	-0.08	0.06	0.06	0.1	0.3
Northwest Territories			0.19	-0.07	-0.03	0.21	0.22	0	-0.41	0.37
Alaska	Total precipitation		-0.38	0.06	-0.23	0.13	-0.07	0.08	-0.2	-0.02
Northwest Territories			-0.16	0.28	0.01	-0.09	0.05	0.06	0	-0.08
Alaska	Relative humidity		0.48	0.12	-0.07	0.22	0.06	0.18	-0.31	0.12
Northwest Territories			-0.11	-0.47	0.11	0.21	-0.11	0.04	0.16	0.04

Table shows correlation of winter and spring meteorology ('Variable') with the number of overwintering flare-ups in Alaska and the Northwest Territories between 2002 and 2018. Results that are significant on a $P < 0.1$ level are shaded light grey, and those on a $P < 0.05$ level dark grey.

Extended Data Table 2 | Comparison of burn scars with and without overwintering fires

Region	Variable	$\mu_{overwinter}$ (± s.d.)	μ_{other} (± s.d.)	*P*
Alaska	First snow-free day	117.9 (± 13.6)	122 (± 12.3)	0.23
Northwest Territories		128.7 (± 9.3)	130.8 (± 12.5)	0.35
Alaska	Vapour Pressure Deficit (VPD)	836.8 (± 176.2)	804.5 (± 210)	0.45
Northwest Territories		1125.8 (± 295.3)	1115.2 (± 246.8)	0.88
Alaska	Fine Fuel Moisture Code (FFMC)	77.7 (± 5)	76.5 (± 5.6)	0.31
Northwest Territories		81.9 (± 3.8)	80.7 (± 4.7)	0.19
Alaska	Duff Moisture Code (DMC)	21.8 (± 8.2)	21.9 (± 10)	0.97
Northwest Territories		34 (± 13.4)	33.6 (± 13.9)	0.9
Alaska	Drought Code (DC)	121.9 (± 36.6)	134.9 (± 39.7)	0.16
Northwest Territories		166.1 (± 35.7)	172.1 (± 46.5)	0.48
Alaska	Initial Spread Index (ISI)	3.8 (± 1.2)	3.8 (± 1.3)	0.92
Northwest Territories		6.1 (± 1.9)	6 (± 1.8)	0.93
Alaska	Buildup Index (BUI)	14.6 (± 5.2)	14.8 (± 6.6)	0.84
Northwest Territories		22.6 (± 8.4)	23 (± 10.3)	0.84
Alaska	Fire Weather Index (FWI)	5.2 (± 2.3)	5.2 (± 2.7)	0.95
Northwest Territories		9.7 (± 4.1)	9.6 (± 4.2)	0.9
Alaska	Daily Severity Rating (DSR)	0.9 (± 0.6)	0.9 (± 0.7)	0.89
Northwest Territories		2.4 (± 1.4)	2.3 (± 1.6)	0.97

The table shows that the average first snow-free day, vapour pressure deficit (VPD) and moisture codes and fire danger indices for days 0 to 50 after the snow melt ('Variable') did not differ significantly for burn scars that produced overwintering fires ('$\mu_{overwinter}$') and those that did not ('μ_{other}'). *P* values are based on the Welch *t*-test. Analysis is based on all (small and large, reported and newly identified) overwintering fires.

Extended Data Table 3 | Effect of spring meteorology on the size of overwintering fires

Region	Variable	$\mu_{small\ (\leq 1\ km2)}$ (± s.d.)	$\mu_{large\ (>1\ km2)}$ (± s.d.)	*P*
Alaska	Vapour Pressure Deficit (VPD)	928.7 (± 483.6)	1138.4 (± 515.3)	0.43
Northwest Territories		1634.2 (± 654.7)	1610.7 (± 528.8)	0.95
Alaska	Fine Fuel Moisture Code (FFMC)	83.5 (± 7.3)	88.2 (± 3.8)	0.14
Northwest Territories		84.8 (± 6.5)	82.9 (± 19.4)	0.68
Alaska	Duff Moisture Code (DMC)	25.3 (± 20.0)	34.8 (± 19.4)	0.36
Northwest Territories		62.0 (± 44.3)	62.8 (± 35.7)	0.97
Alaska	Drought Code (DC)	127.4 (± 54.4)	156.6 (± 41.3)	0.26
Northwest Territories		277.2 (± 87.7)	271.3 (± 68.7)	0.91
Alaska	Initial Spread Index (ISI)	**4.6 (± 3.0)**	**8.7 (± 4.1)**	**0.05**
Northwest Territories		7.1 (± 5.4)	7.5 (± 5.7)	0.90
Alaska	Buildup Index (BUI)	16.4 (± 11.6)	22.4 (± 11.3)	0.32
Northwest Territories		39.6 (± 26.2)	52.5 (± 38.6)	0.49
Alaska	Fire Weather Index (FWI)	**6.1 (± 4.6)**	**13.2 (± 7.3)**	**0.05**
Northwest Territories		15.1 (± 14.1)	18.4 (± 16.7)	0.71
Alaska	Daily Severity Rating (DSR)	**0.9 (± 1.0)**	**3.1 (± 2.7)**	**0.08**
Northwest Territories		4.8 (± 7.0)	7.1 (± 8.6)	0.61

Moisture codes and fire danger indices ('Variable')at the day of detection by the AKFED product for overwintering fires smaller ('$\mu_{small(\leq 1km^2)}$') and larger than 1 km^2 ('$\mu_{large(>1km^2)}$'). Bold numbers represent significant differences at $P < 0.1$.